Electronic Supplementary Material (ESI) for Green Chemistry.

Supporting Information

Uniform Nodules-like Ni_3C/Ni Heterostructure Templated by Metal-organic Frameworks for High-performance Overall Water Splitting

Shumin Wang,[a1] Yi Zhang,[b1] Xiaoyang Deng,[a] Zizai Ma,[cd] Jinping Li,[c] and Xiaoguang Wang*[ac]

[a] Laboratory of Advanced Materials and Energy Electrochemistry, Institute of New Carbon Materials, College of Material Science and Engineering, Taiyuan University of Technology, Taiyuan, 030024, China

[b] Institute of Carbon-Based Thin Film Electronics, Peking University, Shanxi (ICTFE-PKU), Taiyuan, Taiyuan 030012, China

[c] Shanxi Key Laboratory of Gas Energy Efficient and Clean Utilization, Taiyuan University of Technology, Taiyuan, 030024, China

[d] College of Chemistry, Taiyuan University of Technology, Taiyuan, 030024, China

[1] These authors contributed equally

Experimental

1. Materials

Nickel (II) nitrate hexahydrate ($Ni(NO_3)_2 \cdot 6H_2O$, 98.5%), Formic acid (FA, HCOOH, 98.0%) were purchased from Aladdin Industrial Corporation. N, N-dimethylformamide (DMF), acetone, potassium hydroxide (KOH), hydrogen chloride (HCl), acetone and absolute ethanol were purchased from Tianjin Kermel Chemical Reagent Co. Ltd. NF (nickel foam) (void ratio > 98%, ppi: 110) was supplied by Kunshan Jiayisheng Electronics Co. Ltd. Pt/C (20 wt. %), RuO_2 and Nafion (5 wt. %) were purchased from Sigma-Aldrich. All chemicals purchased were reagent grade and without further purification. Ultrapure water (18.2 MΩ cm) was obtained using an UPT-II purification system and used in all experiments.

2. Synthesis of the samples

2.1. Synthesis of Ni-MOF@NF precursor

Firstly, NF was pretreated with 1.0 M HCl to remove surface impurities, and then rinsed with absolute ethanol and deionized water for several times and dried in a vacuum oven at 50 °C for 30 min. The Ni-MOF@NF precursors were synthesized using hydrothermal method. In a typical process, $Ni(NO_3)_2 \cdot 6H_2O$ (1.42 g, 4.875 mmol) and FA (1.25 mL, 32.4 mmol) were dissolved into 20 mL DMF by vigorous stirring for 30 min to acquire a homogenous mixture. Then, the as-prepared solution was transferred into a Teflon-lined stainless steel autoclave with a piece of NF (2×3 cm^2) and maintained at 100 °C in an oven for 12 h. After cooling naturally, the obtained sample was rinsed with DMF and acetone several times, respectively. Eventually, the obtained product on the surface of NF was dried at 50 °C in a vacuum oven for

2 h, which was denoted as Ni-MOF@NF.

2.2. Preparation of Ni_3C/Ni@NF and other contrast samples

The prepared precursor Ni-MOF@NF was placed in a quartz tube furnace, then annealed at 250 °C for 2 h at a heating rate of 2 °C min^{-1} in N_2 atmosphere with total gas flow of 80 mL min^{-1}, which was denoted as Ni_3C/Ni@NF. For morphology and performance comparison, the different calcination time (0.5 h, 2 h and 8 h), were also employed, which were marked as Ni_3C/Ni@NF-0.5 and Ni_3C/Ni@NF-8. Moreover, the samples at various calcination temperatures (250 °C, 350 °C, 450 °C and 550 °C), were also fabricated, which were labeled as Ni_3C/Ni@NF-350, Ni_3C/Ni@NF-450, Ni_3C/Ni@NF-550. In addition, the contrast sample under the H_2 gas atmosphere (mixed atmosphere containing 5% H_2 and 95% N_2), which was marked as Ni@NF. Noted that the mass loading of active materials is ca. 4.0 mg cm^{-2}. The samples of Pt/C/NF and RuO_2/NF were prepared by ink drop coating method. In detail, 5 mg of the Pt/C (20 wt. %) was ultrasonically mixed with isopropyl alcohol (1 mL) and Nafion solution (5 wt. %) (20 μL) to form a well-dispersed catalyst ink. After an ultrasonic treatment for approximately 30 min, the as-obtained suspension ink was deposited on NF with a loading amount equal to the active mass of as-prepared catalysts (4.0 mg cm^{-2}) and dried at ambient temperature. The commercial RuO_2/NF electrode was also made via the same process.

2.3. Materials Characterization

The crystalline structure of Ni-MOF@NF precursors and calcinated products were measured by DX-2700 X-ray diffractometer (XRD) equipped with a Cu Kα radiation source (λ=0.154059 nm) at 40 kV and 30 mA and the diffraction patterns were collected from 5° to

90° at a step size of 0.02°. Thermal gravimetric analysis (TGA) of Ni-MOF powders were carried out using a TG 209 F3 in a nitrogen atmosphere (200 mL min^{-1}) in order to determine the optimum calcination temperature. The microstructure of samples was characterized by scanning electron microscopy (SEM, S-4800, Hitachi), transmission electron microscopy (TEM, JEM-2010F) and high-resolution TEM (HRTEM, JEM-2010F). The chemical state and surface composition of samples were analyzed by X-ray photoelectron spectroscopy (XPS, ESCALAB 250) with Al Kα radiation at 15 kV and 10 mA. The binding energies (BE) were corrected by referencing the C 1s peak at 284.8 eV. X-ray absorption fine structure (XAFS) spectra were collected using an Easy XES150 system (Easy XAFS LLC, USA) and the obtained data were analyzed by the Athena and hama software. The hard X-ray was monochromatized with a Si (551) crystal monochromator and air-cooled tube with Pd outputting at 25 kV and 2 mA. The Brunauer-Emmett-Teller (BET) surface areas were measured using nitrogen adsorption isotherms at 77 K (3H-2000 PM2). The corresponding pore size distribution was calculated from the adsorption branches of isotherms via the Barrett-Joyner-Halenda method. The contact angles were tested by a SL200B analyzer (Solon Tech. (Shanghai) Co., Ltd.) to evaluate the surface wettability. When the 2 μL of 1.0 M KOH solution was dropped on the sample surface, the equipped camera system would capture a photo to determine the contact angle. Raman spectra analysis (LabRam HR Evolution, λ = 532 nm) was adopted to distinguish the characteristic vibrational modes of the synthesized materials. In all tests, only the SEM and contact angles test is performed for the total Ni_3C/Ni@NF electrode. For the SEM and contact angles tests, the samples grown on NF was characterized to observe the specific morphology. For the other tests (including XRD, TEM, XPS, XAFS, BET and Raman spectra), the Ni_3C/Ni

powders were carefully scraped off from the surface of Ni_3C/Ni@NF sample.

2.4. Electrochemical measurements

All the electrochemical measurements were carried out in alkali solution (1.0 M KOH) on a CS-350 electrochemical workstation at a typical three-electrode system equipped with a high-purity graphite rod as counter electrode, a Hg/HgO (1.0 M KOH) as reference electrode, and as-prepared samples as working electrode, respectively. Meanwhile, the catalytic performance of pristine Ni foam was also estimated as the cathode and anode. Before each electrochemical measurement, the electrolytes were deaerated by bubbling of N_2 for 30 min to avoid any possible occurrence of oxygen reduction. Before evaluating the HER and OER activity, all catalysts were activated by 20 cyclic voltammetry (CV) cycles across the potential window at a scan rate of 20 mV s^{-1} to reach a steady state. The linear-sweep voltammetry (LSV) were performed at a scan rate of 5 mV s^{-1} for HER and 2 mV s^{-1} for OER in 1.0 M KOH solution with 80% iR compensation.[1] All tested potentials were normalized to reversible hydrogen electrode (RHE) via the Nernst equation (1):

$$E\,(RHE) = E\,(Hg/HgO) + 0.098 + 0.059 \times pH - 80\%iR_s \quad (1)$$

where E (RHE) is the potential vs. RHE, E (Hg/HgO) is the tested potential, and R_s is solution resistance.

The Tafel plots were calculated based on the equation (2):

$$\eta = b \log j + a \quad (2)$$

Where η, b and j are the overpotential, Tafel slope and current density, respectively. Electrochemical impedance spectra (EIS) were performed in the frequency range from 0.1 Hz

to100 kHz at potentials of –0.066 V (vs. RHE) for HER and 1.574 V (vs. RHE) for OER with a 10 mV sinusoidal perturbation. Furthermore, to evaluate the electrochemical surface area (ECSA) of these electrodes, double-layer capacitance measurements (C_{dl}) were carried out in the potential region from 0.054 V to 0.154 V (vs. RHE) for HER performance and 0.924 V to 1.024 V (vs. RHE) for OER performance without faradaic process from the CV curves at different scan rates (20, 40, 60, 80, 100 and 120 mV s^{-1}). The corresponding specific C_{dl} values were obtained by calculating the slope by plotting Δj vs. scan rates where Δj = |janode − jcathode|/2.[2] In general, the ECSA is calculated based on the following equation (3):

$$ECSA = \frac{C_{dl}}{C_s} \tag{3}$$

Where C_s is the specific capacitance of the sample or the capacitance of an atomically smooth planar surface of the material per unit area under identical electrolyte conditions. Generally, due to the specific capacitance of atomically smooth planar surface with a real surface area of 1.0 cm^2, the specific capacitance (C_s) is calculated within 20-60 µF cm^{-2} in alkaline media. In this study, 40 µF cm^{-2} is used as the general specific capacitance of C_s in 1.0 M alkaline media reported in many previous literatures.[3, 4] In addition, the Faradaic efficiency (FE) was determined by monitoring gases evolution (H_2 and O_2) under the current density of 10 mA cm^{-2} in a sealed electrolytic cell. In detail, the amount of generated gases during bulk electrolysis was quantified by gas chromatography (GC, 8860 GC System, carrier gas: Ar; chromatographic column: 5 Å molecular sieve column; detector: TCD). Before each measurement, the electrolyte was bubbled with Ar for 30 min.

In order to investigate the effect of ECSA on the electrocatalytic performance, the HER and OER curves were normalized by ECSAs. The ECSA-normalized current density for the catalysts was calculated by the following equation:

$$\text{Current density}_{ECSA} = j \times C_s / C_{dl} \quad (4)$$

2.5. DFT calculations

The theoretical calculations were performed via density functional theory (DFT) by the Vienna Ab-initio Simulation Package (VASP).[5] In this work, the core and valence electrons were represented by the projector augmented wave (PAW) method and plane-wave basis functions with a kinetic energy cut-off of 450 eV. The convergence threshold for structural optimization was set as 10^{-5} eV in energy and –0.05 eV in force. In this work, the Brillouin zone was sampled with the Monkhorst-Pack scheme. Monkhorst-Pack k-point setups were 3×3×3 and 3×3×1 for bulk and slab geometry optimization, respectively.

The hydrogen adsorption Gibbs free energy ΔG_H can be achieved as follows:

$$\Delta G_H = \Delta E_H + \Delta ZPE - T\Delta S_H \quad (5)$$

Where ΔE_H represents the adsorption energy of H. ΔZPE and $T\Delta S_H$ represent the difference of the zero-point energy and entropy between the hydrogen adsorbed state and the gas phase H_2. Moreover, the overall contribution can be rewritten as:

$$\Delta G_H = \Delta E_H + 0.24 = E_{(surf+H)} - E_{(surf)} - 1/2 E_{(H_2)} + 0.24 \quad (6)$$

The OER performance of the catalysts was determined by the relative energy of the intermediates OH, O, OOH and O_2 in alkaline environments:

$$* + H_2O \rightarrow *OH + (H^+ + e^-) \quad (7)$$

$$*OH \rightarrow *O + (H^+ + e^-) \quad (8)$$

$$*O + H_2O \rightarrow *OOH + (H^+ + e^-) \quad (9)$$

$$*OOH \rightarrow O_2 + (H+ + e^-) \quad (10)$$

where * represents adsorption sites. The relative energy of each step is obtained by

$$\text{Relative energy} = \Delta E_H + \Delta ZPE - T\Delta S \quad (11)$$

where ΔE_H is the calculated total energy difference, ΔZPE and TΔS is zero-point energy correction and entropy difference, respectively.

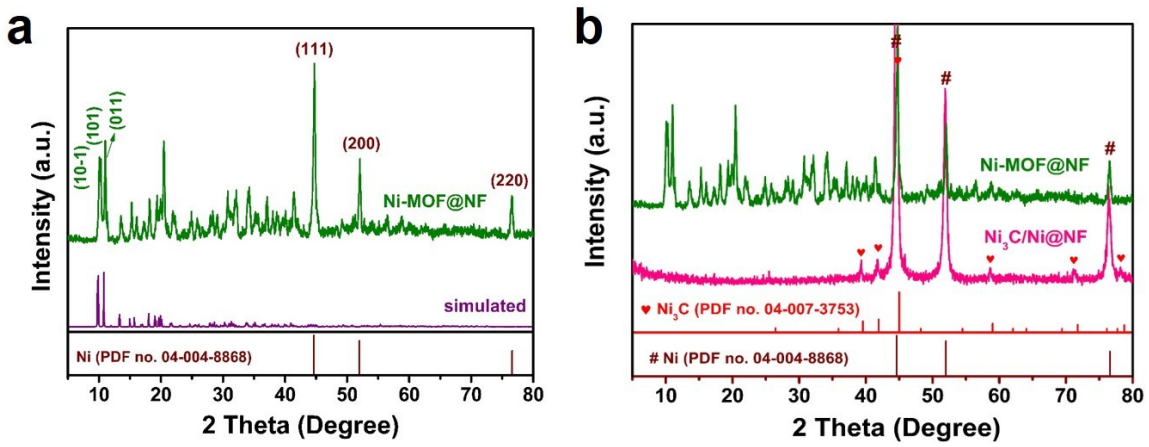

Fig. S1. XRD patterns of (a)Ni-MOF@NF precursor and (b) Comparison of Ni_3C/Ni@NF and Ni-MOF@NF precursor.

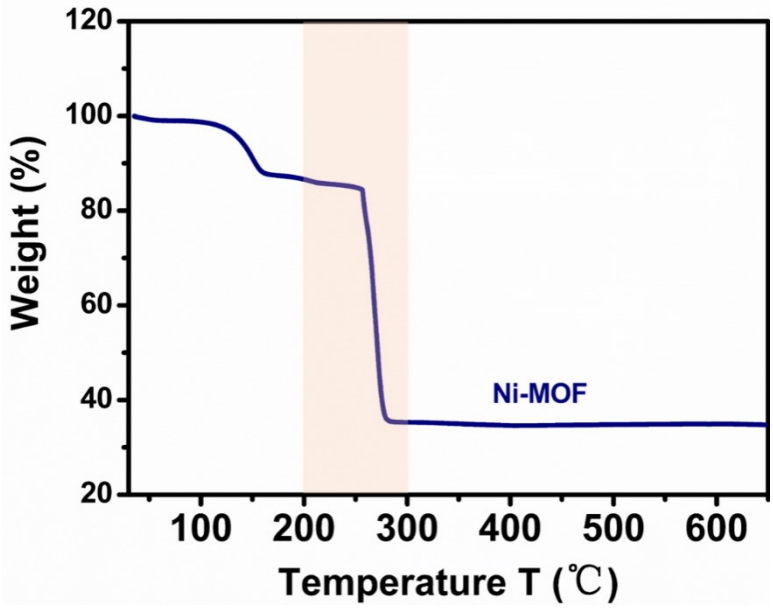

Fig. S2. Thermogravimetric analysis (TGA) of Ni-MOF in nitrogen atmosphere.

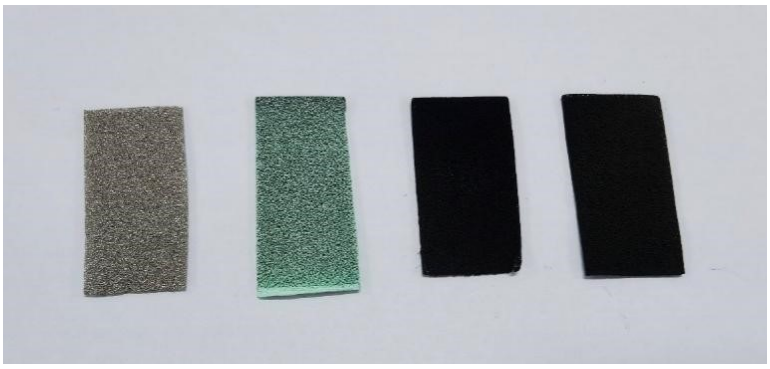

Fig. S3. Photographs of the samples. From left to right: bare NF, Ni-MOF@NF precursor, Ni_3C/Ni@NF and Ni@NF.

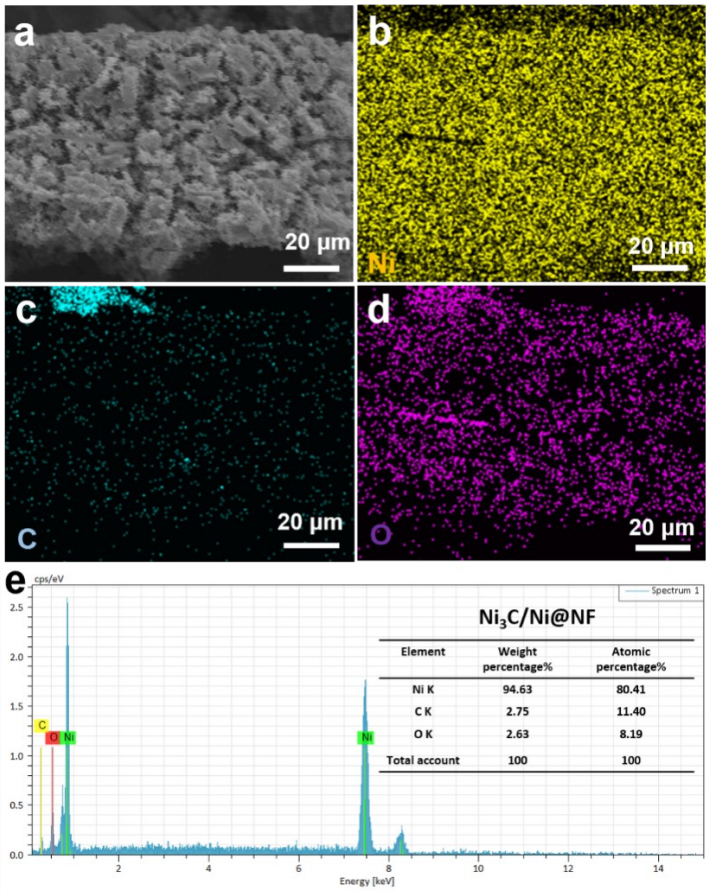

Fig. S4. EDX mapping and elemental analysis of Ni_3C/Ni@NF.

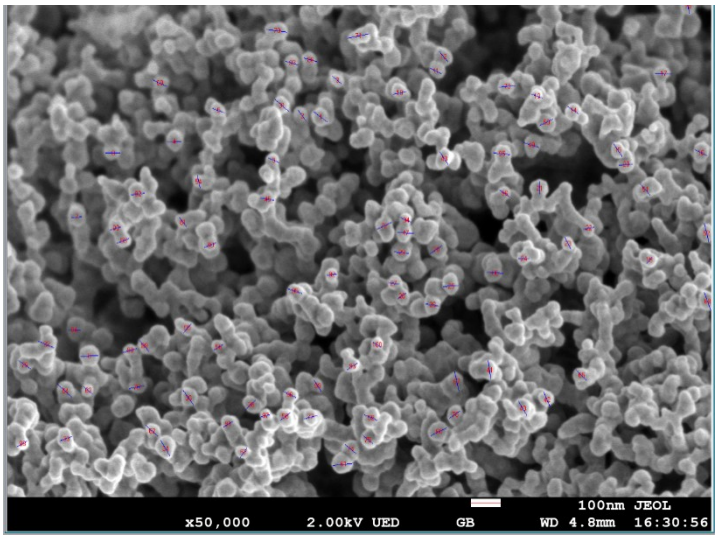

Fig. S5. SEM image for standardization of particle size of Ni_3C/Ni@NF.

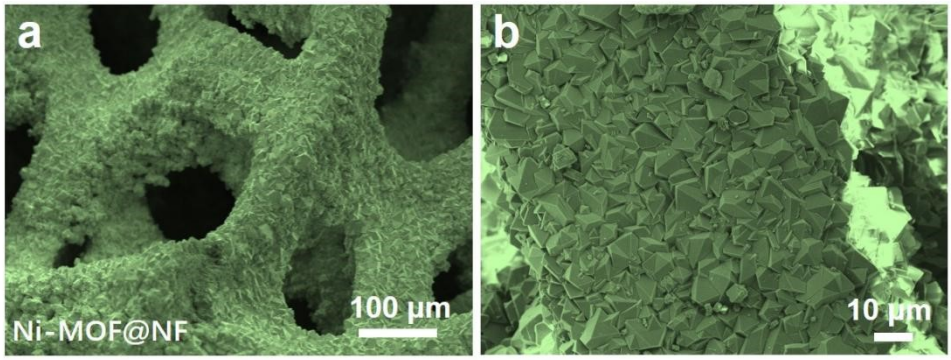

Fig. S6. SEM images of Ni-MOF@NF precursor.

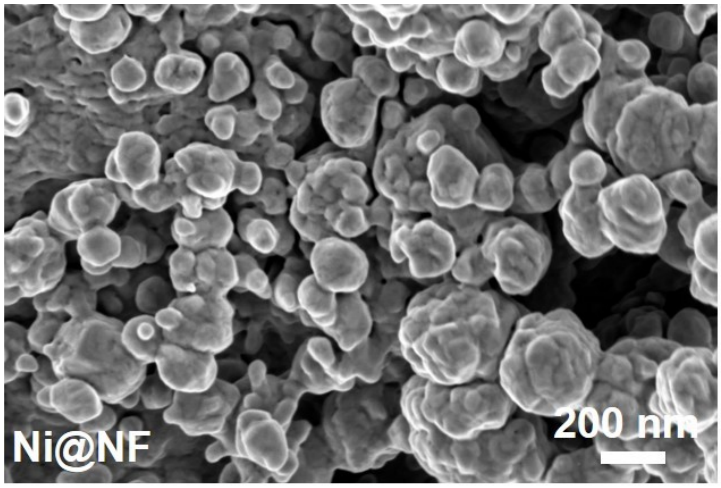

Fig. S7. SEM images of Ni@NF.

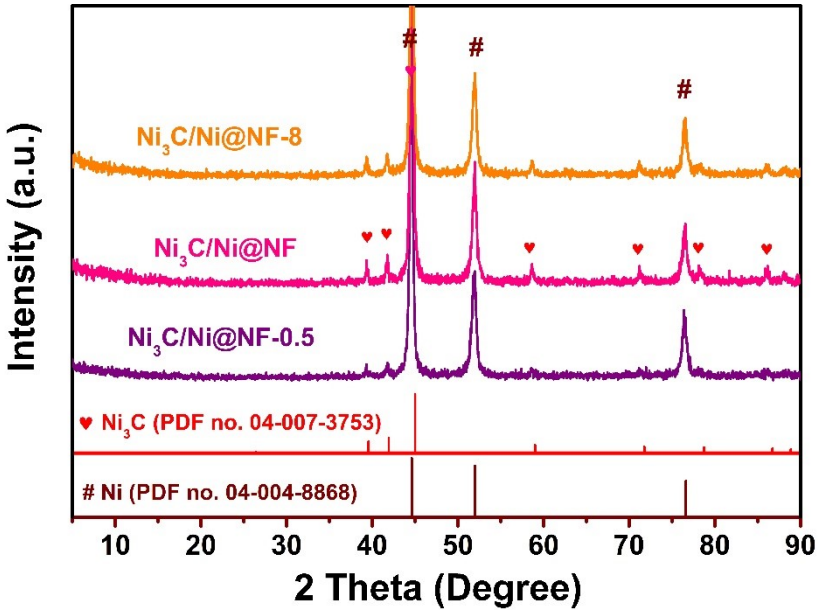

Fig. S8. XRD patterns of the calcinated product of Ni-MOF@NF at 250 °C in nitrogen for different time (0.5, 2 and 8 h).

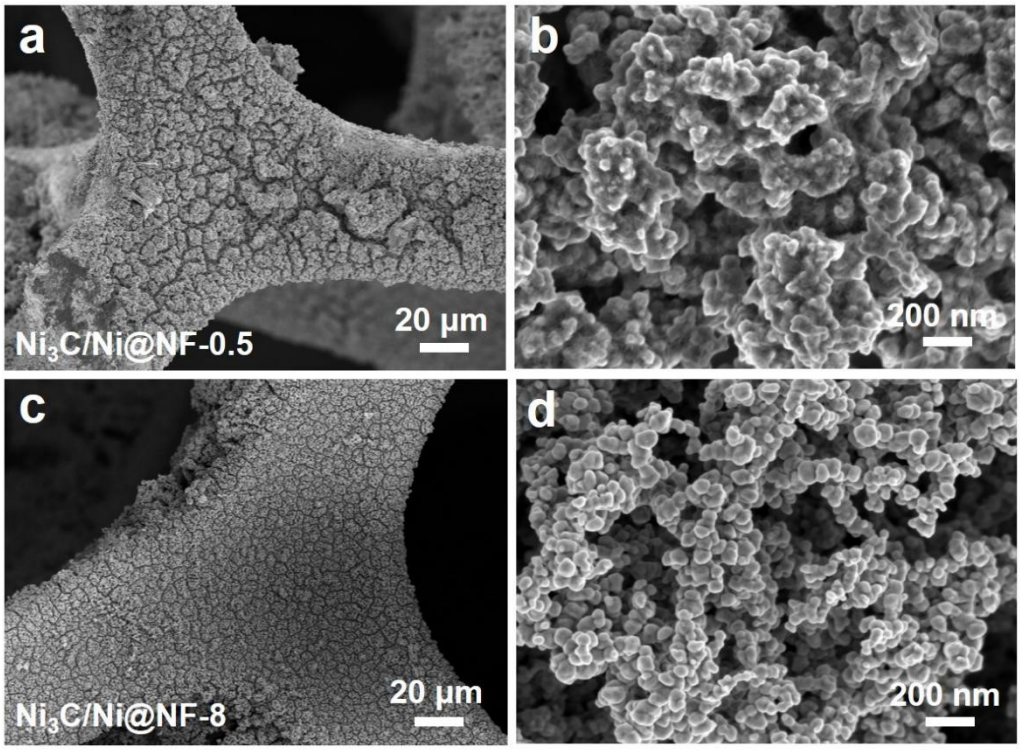

Fig. S9. SEM images of the calcinated products. (a, b) Ni_3C/Ni@NF-0.5 and (c, d) Ni_3C/Ni@NF-8.

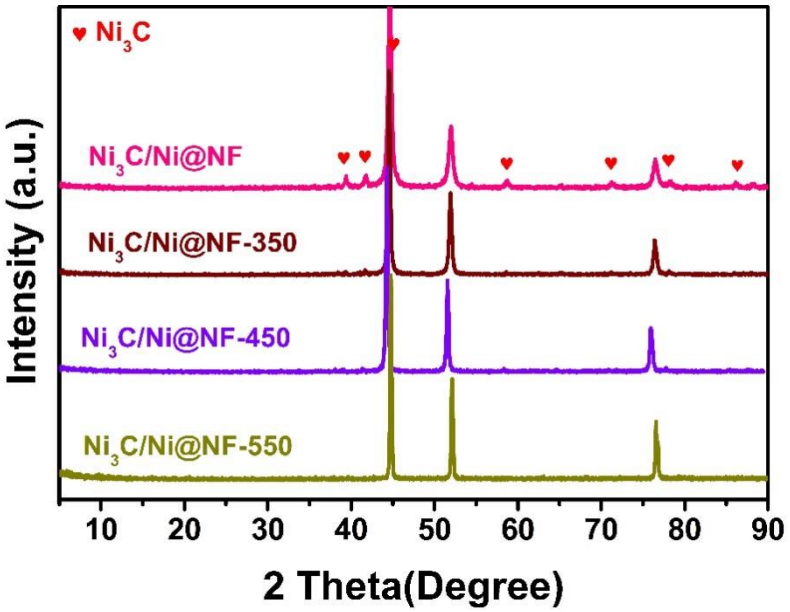

Fig. S10. XRD patterns of the calcinated products of Ni-MOF@NF in nitrogen for 2 h at different temperatures (250, 350, 450 and 550 °C).

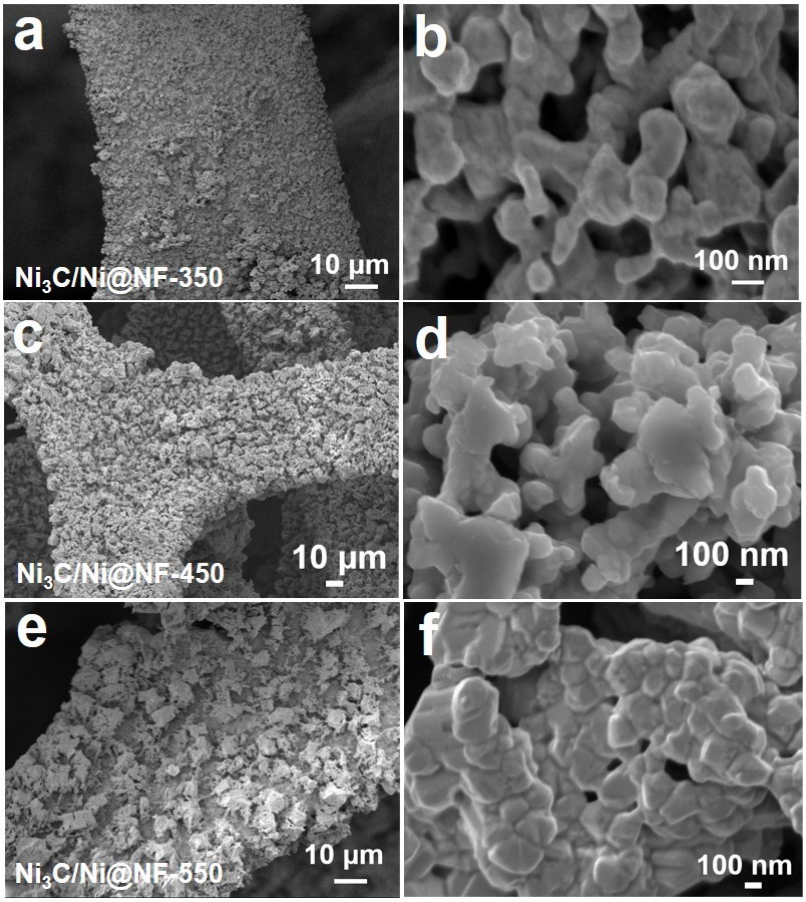

Fig. S11. SEM images of the calcinated products. (a, b) Ni_3C/Ni@NF-350. (c, d) Ni_3C/Ni@NF-450. (e, f) Ni_3C/Ni@NF-550.

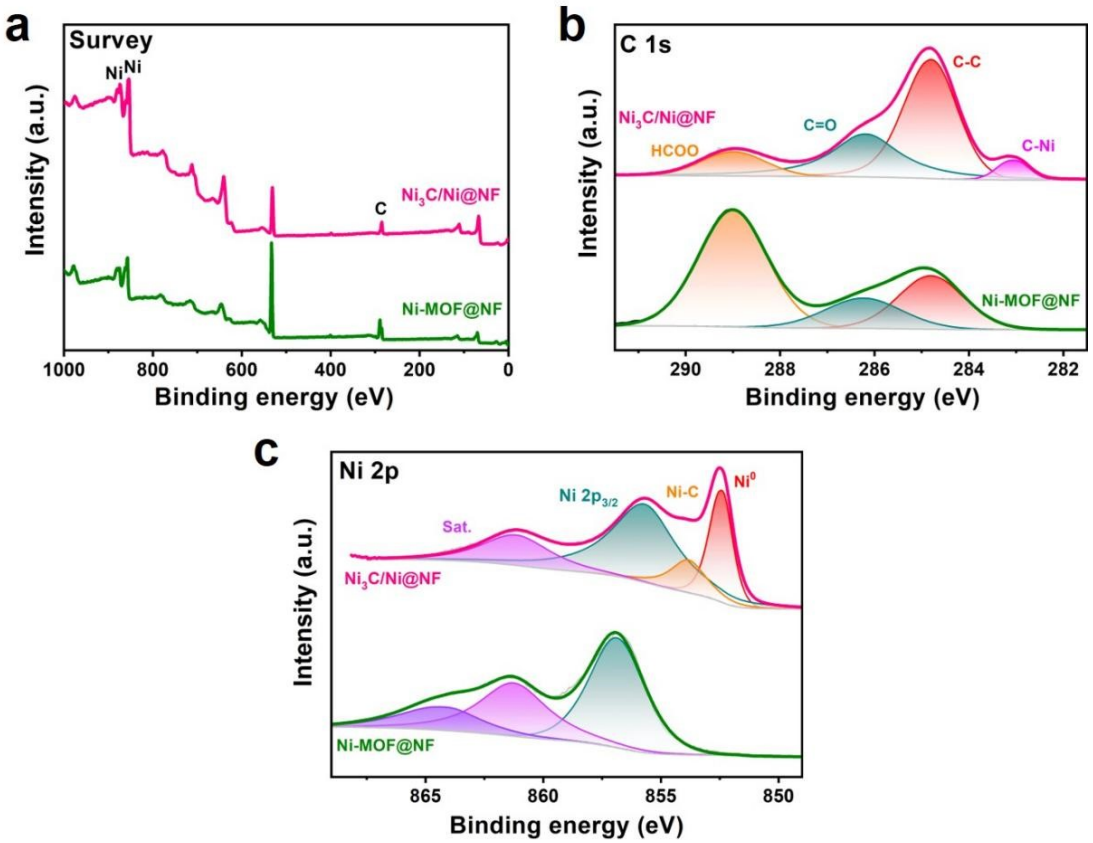

Fig. S12. XPS spectra for Ni_3C/Ni@NF and Ni-MOF@NF precursor scraped from Ni foam. (a) XPS survey. (b) C1s and (c) Ni 2p region.

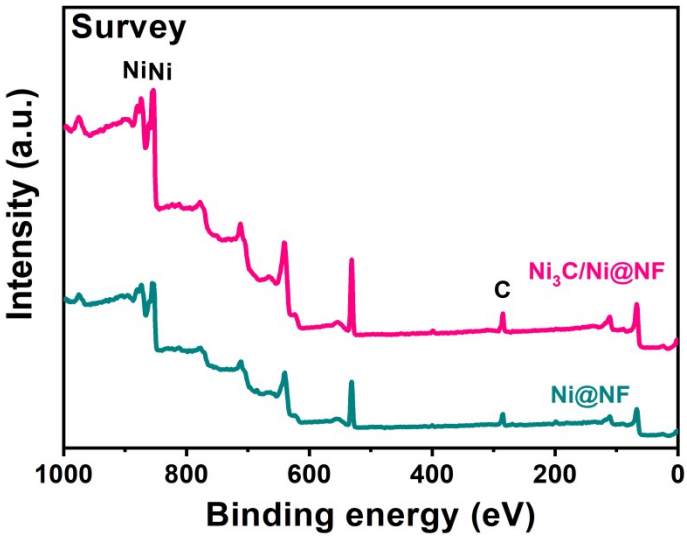

Fig. S13. Survey XPS spectra of Ni_3C/Ni@NF and Ni@NF.

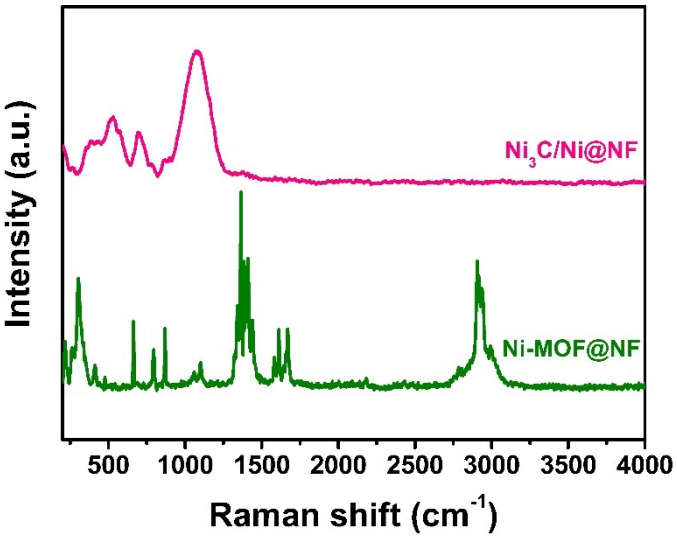

Fig. S14. Raman spectra of Ni_3C/Ni@NF and Ni-MOF@NF precursor.

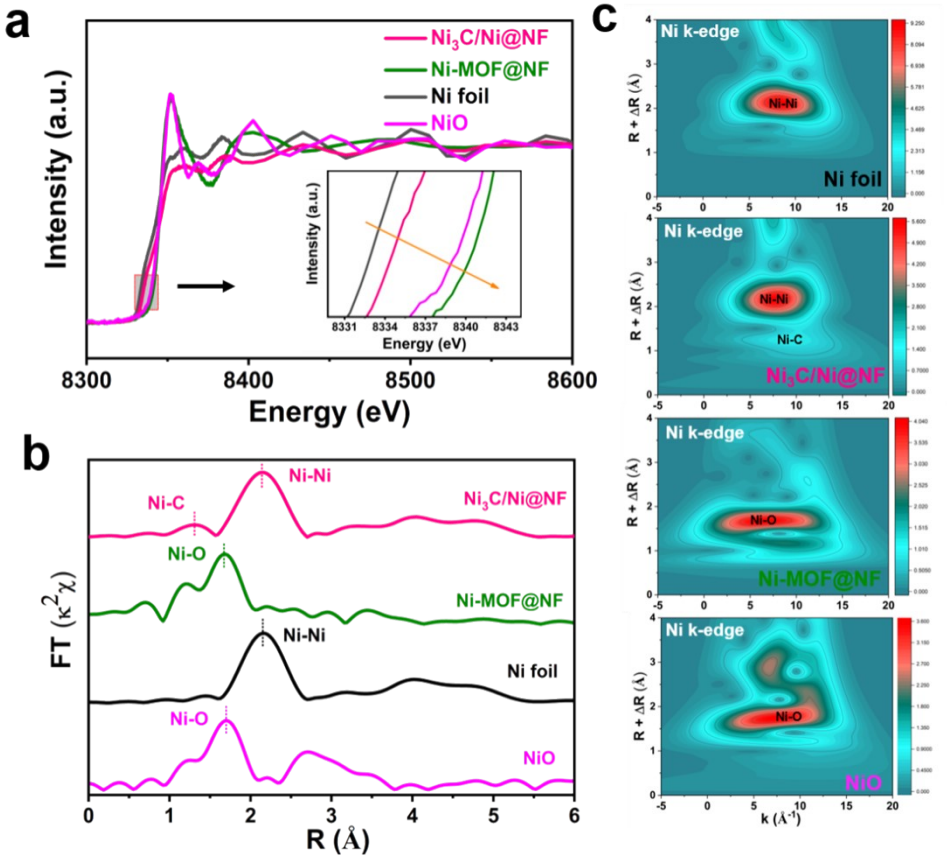

Fig. S15. (a) The normalized Ni K-edge XANES spectra. (b) Corresponding FT-EXAFS spectra. (c) WT contour plots of Ni K-edge at R space of Ni_3C/Ni@NF, Ni-MOF@NF, Ni foil and NiO.

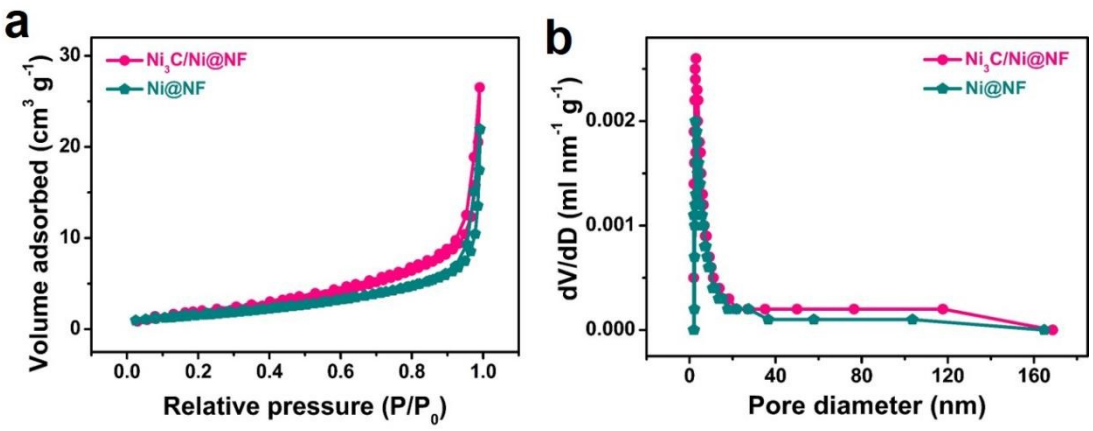

Fig. S16. (a) N_2 adsorption/desorption isotherms and (b) pore size distribution of Ni_3C/Ni@NF and Ni@NF.

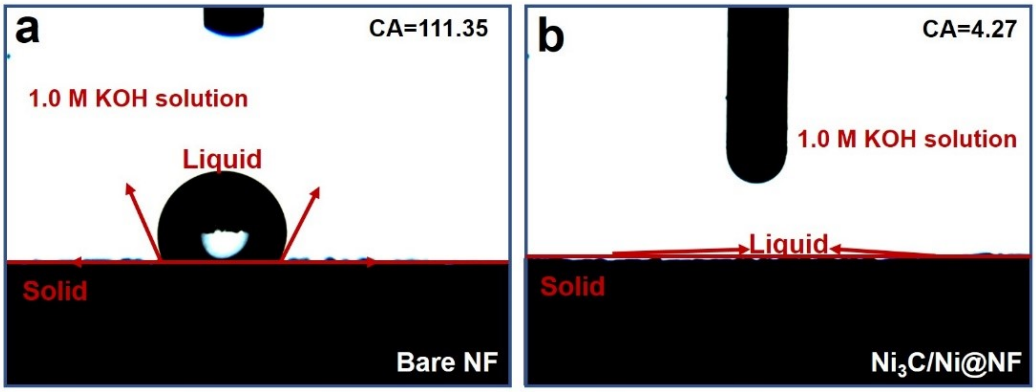

Fig. S17. Contact angles of (a) bare NF and (h) Ni_3C/Ni@NF.

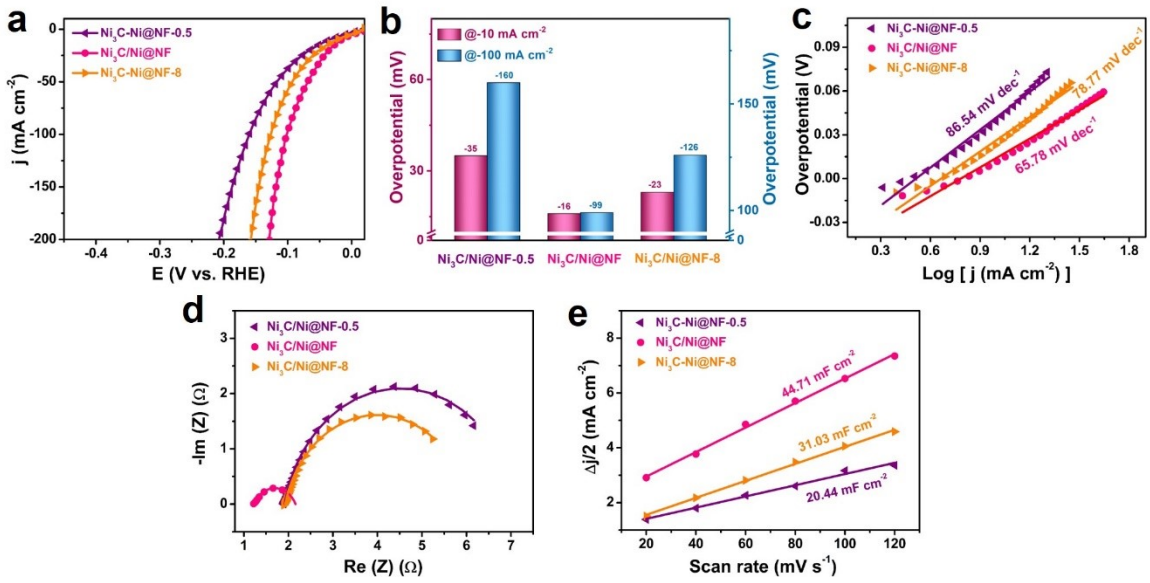

Fig. S18. (a) HER polarization curves of as-prepared catalysts with different calcination time (Ni_3C/Ni@NF-0.5, Ni_3C/Ni@NF and Ni_3C/Ni@NF-8). (b) Bar graph of overpotentials (η) at 10 and 100 mA cm^{-2}. (c) Tafel plots. (d) Nyquist plots. Scatters: experimental data; lines: fitted curves. (e) C_{dl} plots.

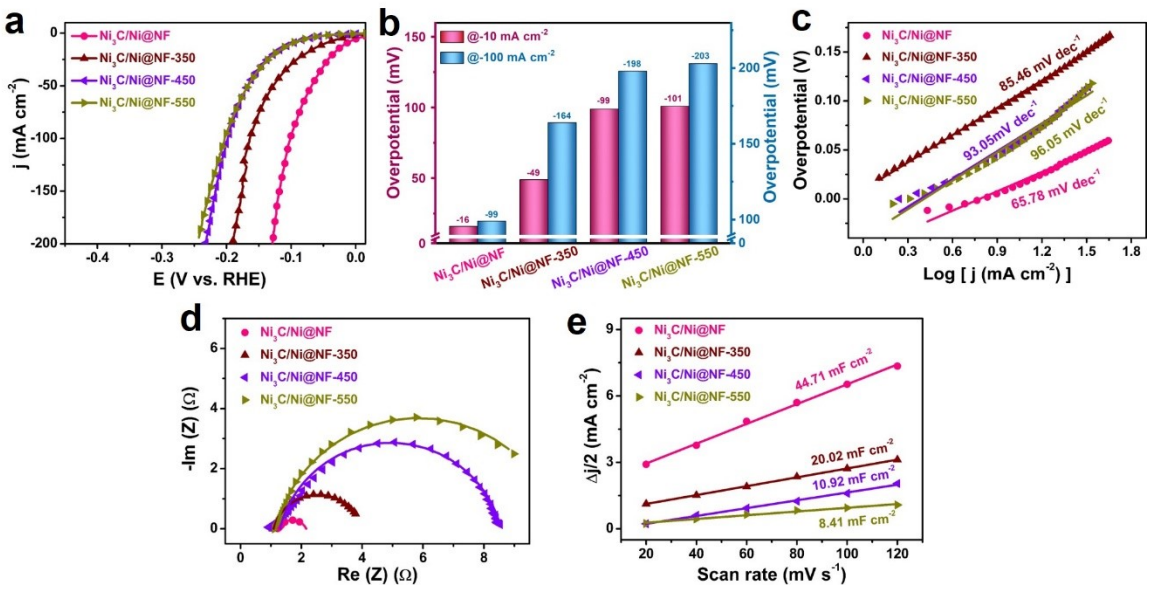

Fig. S19. (a) HER polarization curves of as-prepared catalysts at different calcination temperatures (Ni_3C/Ni@NF, Ni_3C/Ni@NF-350, Ni_3C/Ni@NF-450 and Ni_3C/Ni@NF-550). (b) Bar graph of overpotentials (η) at 10 and 100 mA cm^{-2}. (c) Tafel plots. (d) Nyquist plots. Scatters: experimental data; lines: fitted curves. (e) C_{dl} plots.

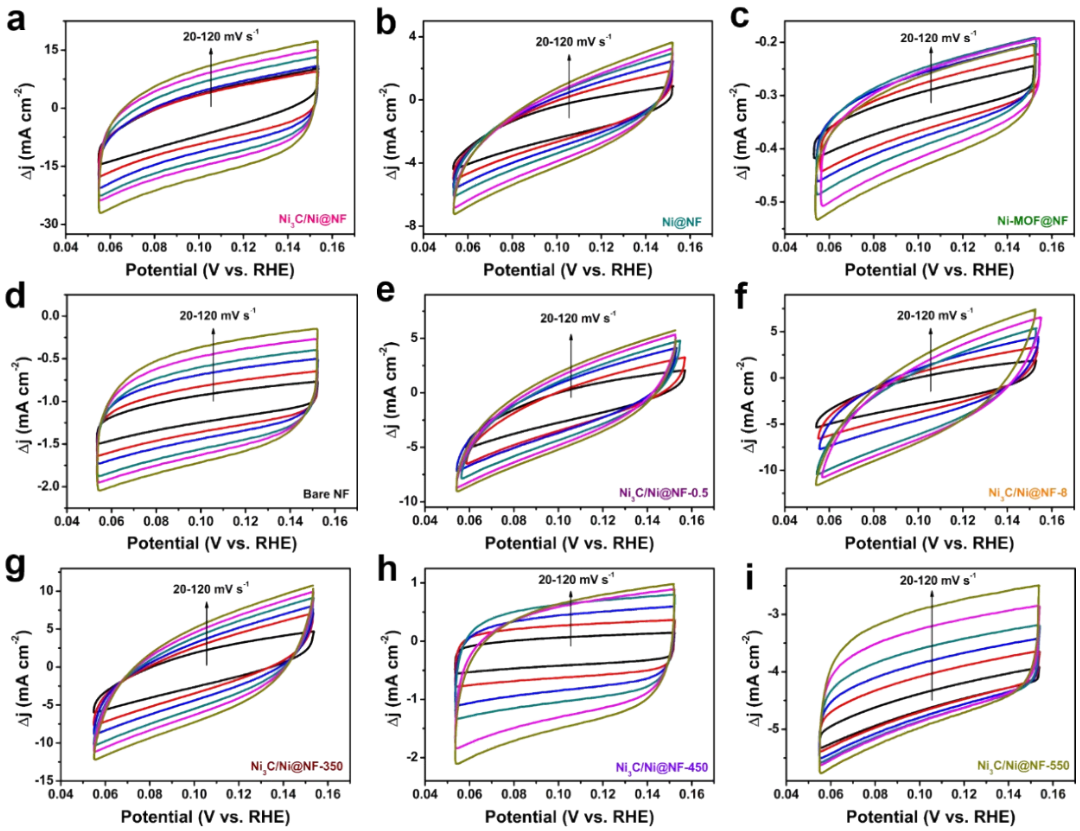

Fig. S20. Cyclic voltammograms of catalysts at different scan rates from 20 mV s^{-1} to 120 mV s^{-1} in 1.0 M KOH for HER.

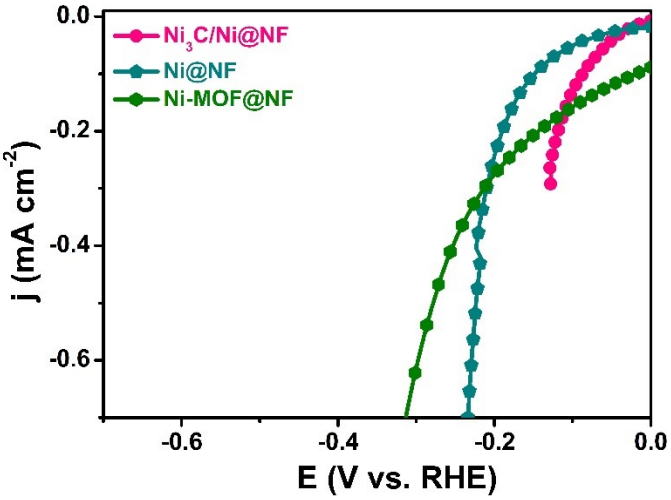

Fig. S21. ECSA-normalized LSV curves for Ni_3C/Ni@NF, Ni@NF and Ni-MOF@NF toward the HER.

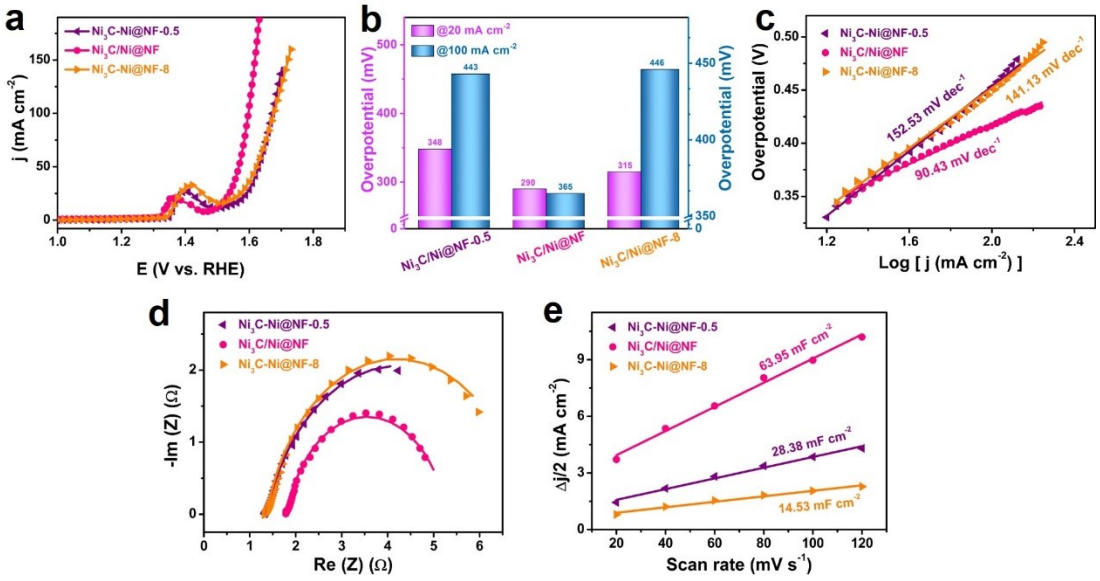

Fig. S22. (a) OER polarization curves of as-prepared catalysts with different calcination time (Ni_3C/Ni@NF-0.5, Ni_3C/Ni@NF and Ni_3C/Ni@NF-8). (b) Bar graph of the overpotentials (η) at 20 and 100 mA cm^{-2}. (c) Tafel plots. (d) Nyquist plots. Scatters: experimental data; lines: fitted curves. (e) C_{dl} plots.

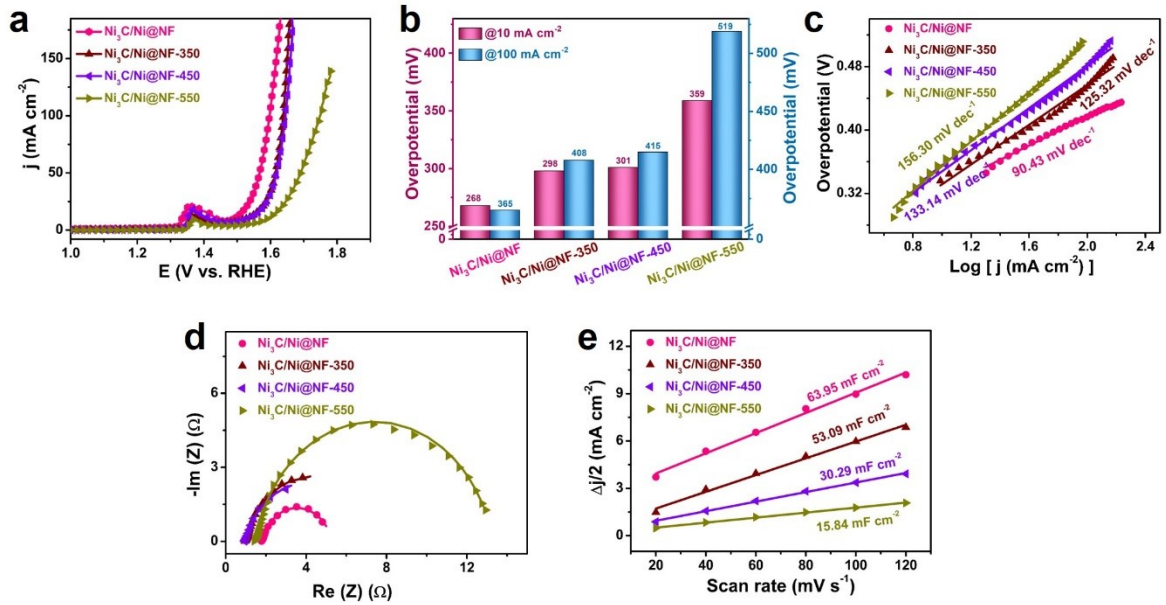

Fig. S23. (a) OER polarization curves of as-prepared catalysts at different calcination temperatures (Ni_3C/Ni@NF, Ni_3C/Ni@NF-350, Ni_3C/Ni@NF-450 and Ni_3C/Ni@NF-550). (b) Bar graph of the overpotentials (η) at 10 and 100 mA cm^{-2}. (c) Tafel plots. (d) Nyquist plots. Scatters: experimental data; lines: fitted curves. (e) C_{dl} plots.

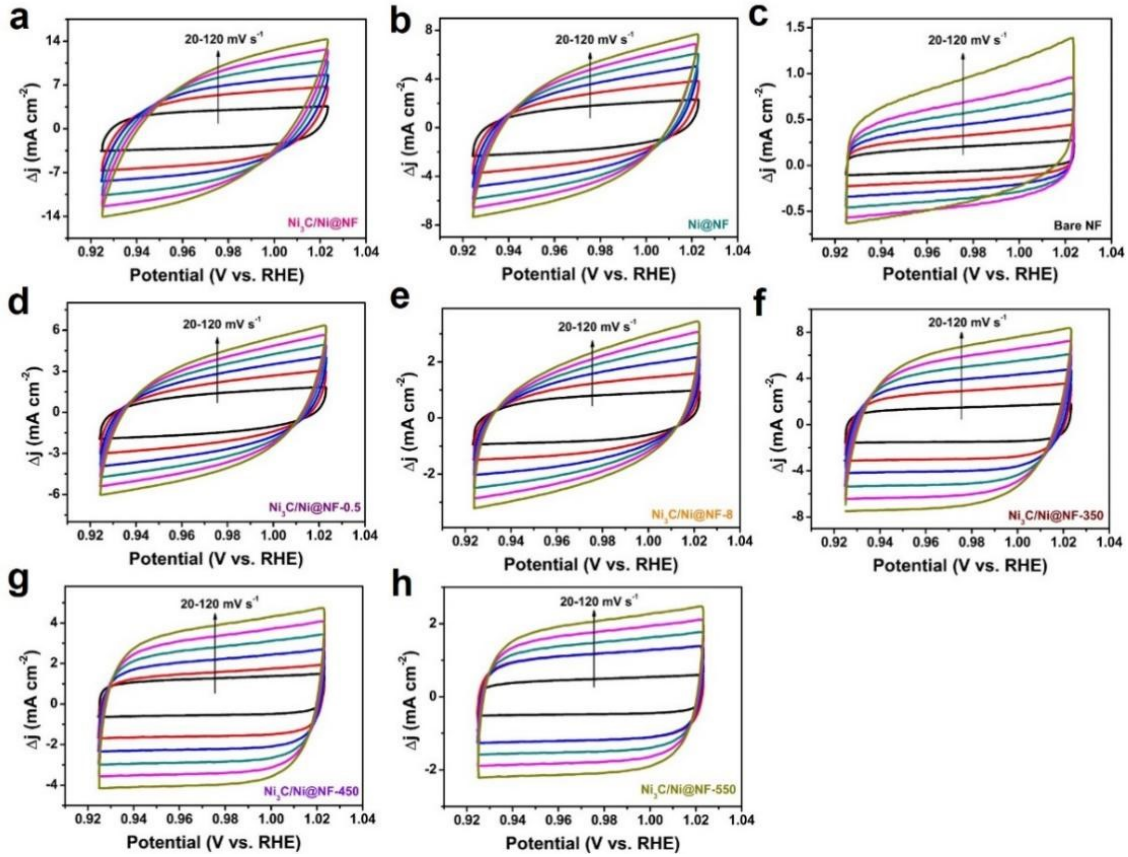

Fig. S24. Cyclic voltammograms of catalysts at different scan rates from 20 mV s^{-1} to 120 mV s^{-1} in 1.0 M KOH for OER.

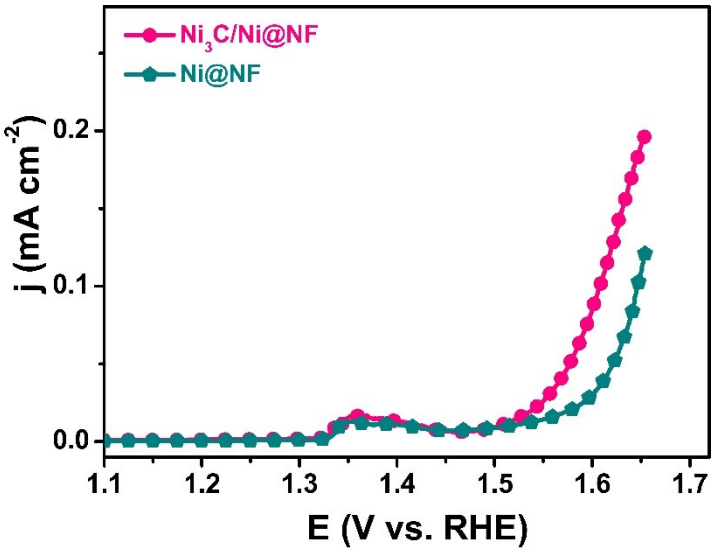

Fig. S25. ECSA-normalized LSV curves for Ni_3C/Ni@NF and Ni@NF toward the OER.

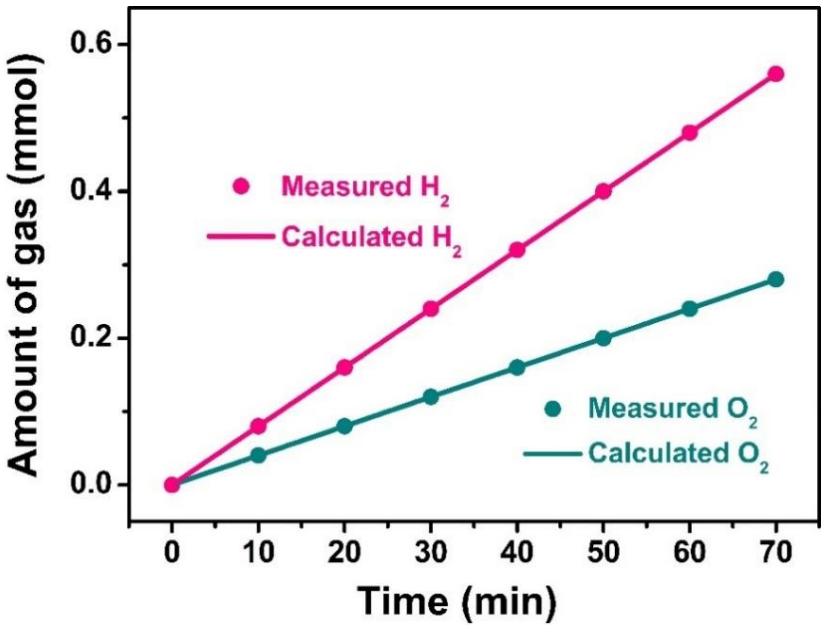

Fig. S26. The amount of gas theoretically calculated and experimentally measured versus time for Ni_3C/Ni@NF.

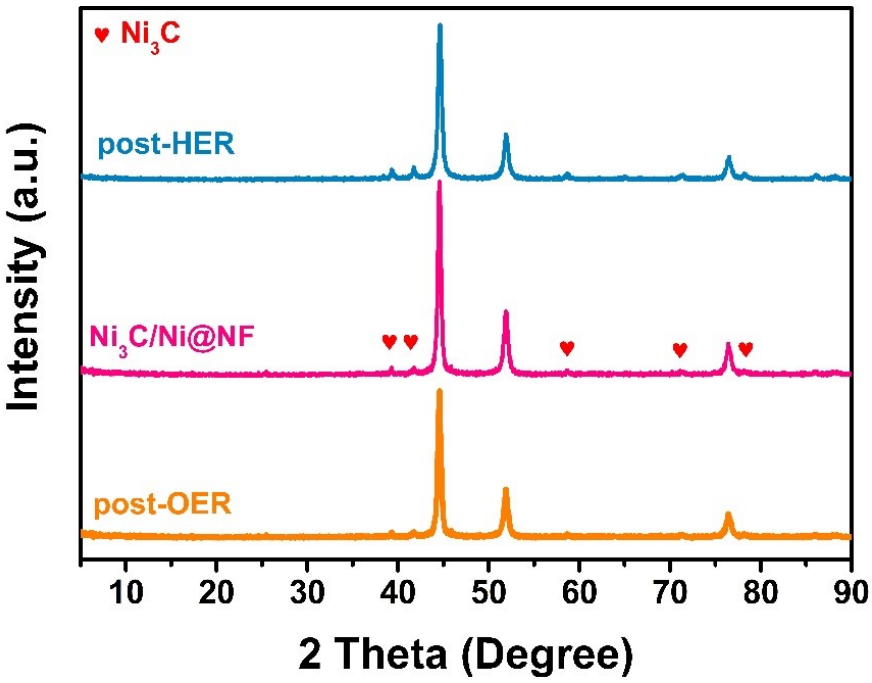

Fig. S27. XRD for the initial Ni_3C/Ni@NF, post-HER and post-OER samples scraped from Ni foam.

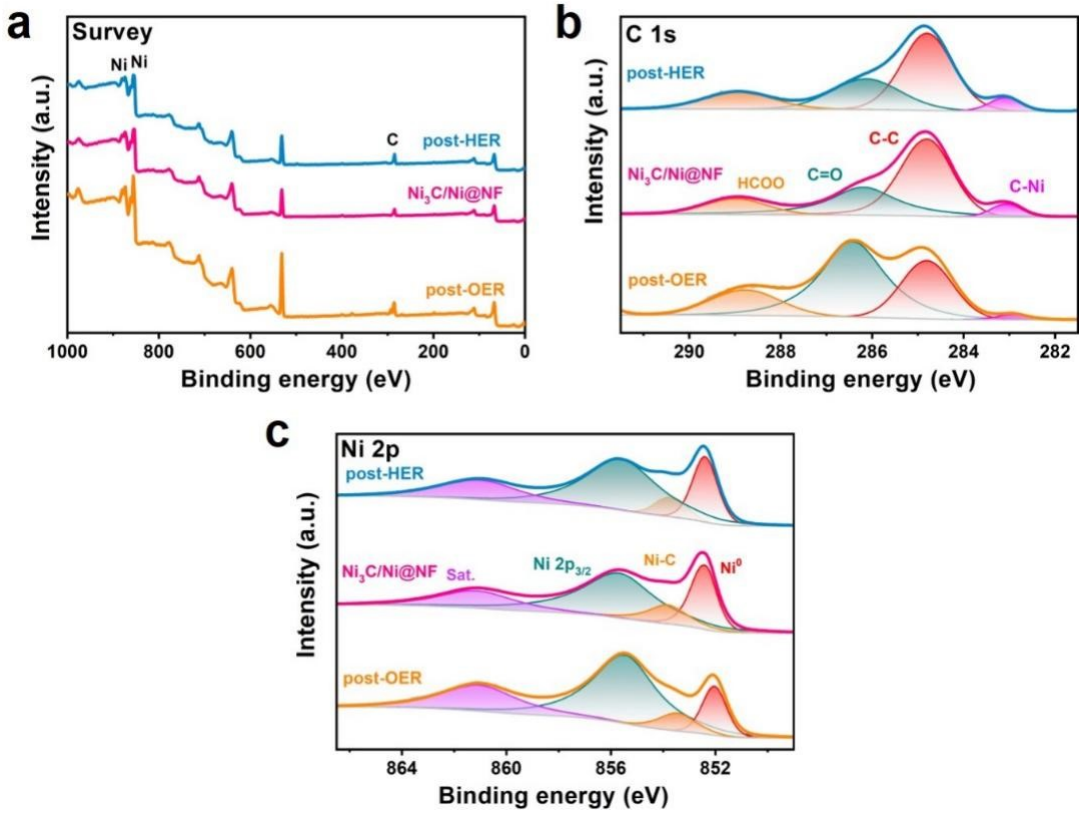

Fig. S28. XPS spectra for initial Ni_3C/Ni@NF, post-HER and post-OER samples scraped from Ni foam. (a) XPS survey. (b) C 1s and (c) Ni 2p region.

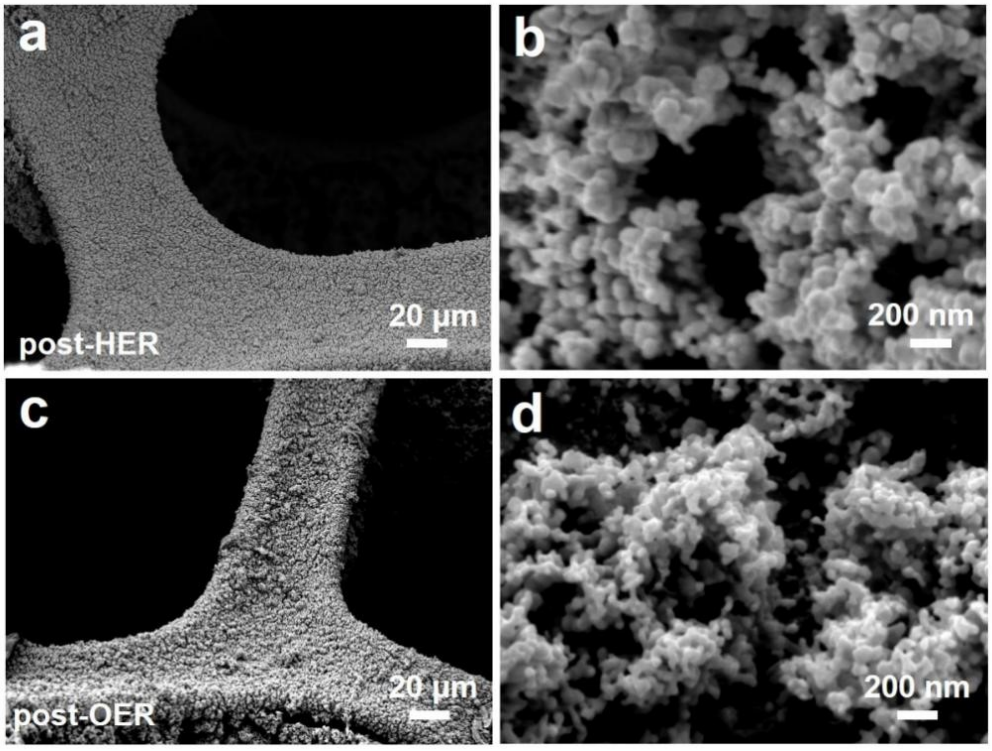

Fig. S29. SEM images for (a, b) post-HER and (c, d) post-OER samples for Ni_3C/Ni@NF.

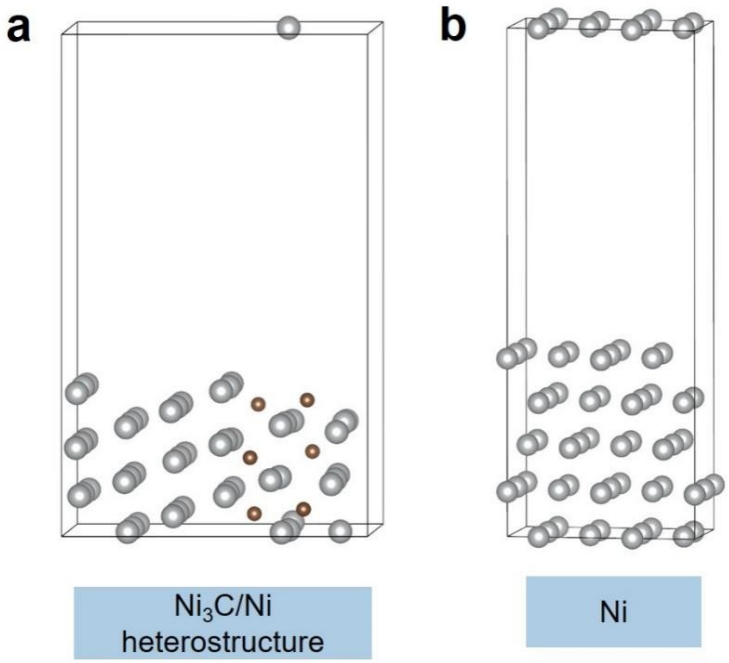

Fig. S30. Models of (a) Ni_3C/Ni heterostructure and (b) Ni.

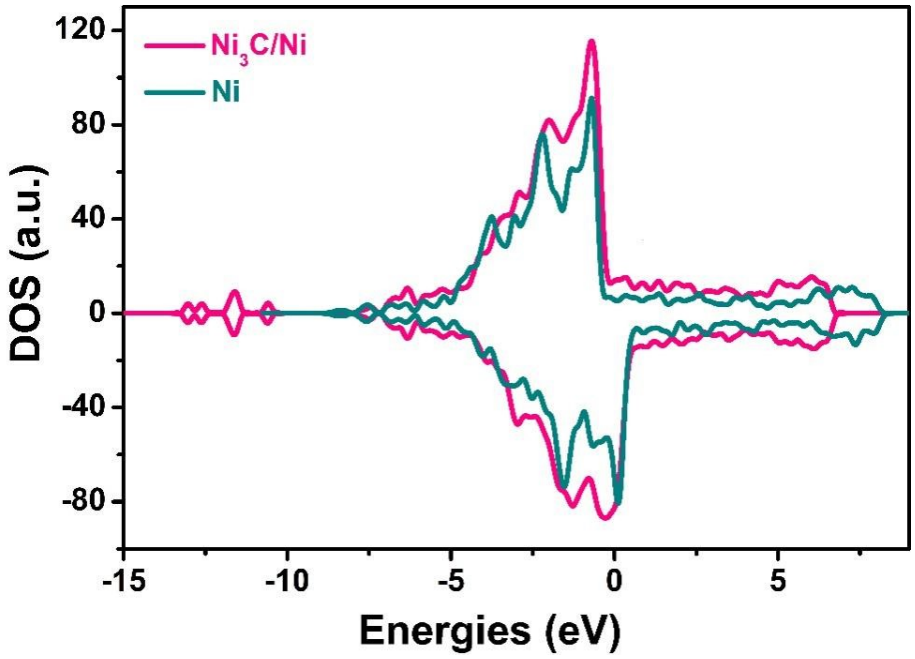

Fig. S31. Total density of states (DOS) of Ni_3C/Ni and Ni.

Table S1. Comparison of Tafel slope and required overpotential at current density of 10 mA cm^{-2} (η_{10}) for Ni_3C/Ni@NF with many of reported state-of-the-art noble-metal-free HER electrocatalysts in 1.0 M KOH.

Catalysts	**η_{10} (mV)**	**Tafel slope (mV dec^{-1})**	**Reference**
Ni_3C/Ni@NF	16	65.78	This work
FeCoMnNi-MOF-74/NF	108	72.89	6
0.4-Co_2P/Ni_xP_y@NF	81	86	7
Cr−Ni NHs	75	72	8
CoFeP TPAs/Ni	43	30	9
Ir@Ni/NiO	54.7	71.5	10
CoP/NF	41.1	65.3	11
MnxFeyNi-MOF-74	99	103.8	12
V_8C_7/CoP	119	109	13
Ni/C-H_2-700	120	121	14

Table S2. EIS parameters (R_s and R_{ct}) of a series of catalysts at a controlled-potential of −0.066 V vs. RHE for HER.

Catalysts	R_s (Ω)	R_{ct} (Ω)
Ni_3C/Ni@NF	1.335	0.92
Ni@NF	1.169	2.19
Ni-MOF@NF	1434	99.74
Ni_3C/Ni@NF-0.5	1.916	5.19
Ni_3C/Ni@NF-8	1.929	4.13
Ni_3C/Ni@NF-350	1.087	2.93
Ni_3C/Ni@NF-450	1.300	7.26
Ni_3C/Ni@NF-550	1.159	9.35
Pt/C/NF	1.085	1.68
Bare NF	1.411	95.83

Table S3. Comparison of double layer capacitance (C_{dl}) and electrochemical active surface area (ECSA) of as-synthesized samples for HER.

Catalysts	C_{dl} (mF cm^{-2})	ECSA (cm^2)
Ni_3C/Ni@NF	44.71	1117.75
Ni@NF	14.81	370.25
Ni-MOF@NF	0.59	14.75
Ni_3C/Ni@NF-0.5	20.44	511.00
Ni_3C/Ni@NF-8	31.03	775.75
Ni_3C/Ni@NF-350	20.02	500.50
Ni_3C/Ni@NF-450	10.92	27.30
Ni_3C/Ni@NF-550	8.41	210.25
Bare NF	1.03	25.75

Table S4. Comparison of Tafel slope and required overpotential at current density of 10 mA cm^{-2} (η_{10}) for Ni_3C/Ni@NF with many of reported state-of-the-art noble-metal-free OER electrocatalysts in 1.0 M KOH.

Catalysts	η_{10} (mV)	Tafel slope (mV dec^{-1})	Reference
Ni_3C/Ni@NF	268	90.43	This work
VOB-Co_3O_4/NF	315	112.5	3
Co_3O_4@Ni_2P	270	67	15
DLD-FeCoP@CNT	286	39.6	16
CoNi/NC-YS	292	53.8	17
NiFe-S-13@CNFs	270	44.4	18
$Mo_{0.2}$-Co-O NSs	276	63	19
$Fe_{0.6}Co_{0.4}P$@O	346	36	20
Ni-CoP-2	306	50	21
Ni/Fe_3O_4	296	61	22

Table S5. EIS parameters (R_s and R_{ct}) of a series of catalysts at a controlled-potential of 1.574 V vs. RHE for OER.

Catalysts	R_s (Ω)	R_{ct} (Ω)
Ni_3C/Ni@NF	1.811	3.48
Ni@NF	1374	5.61
Ni_3C/Ni@NF-0.5	1.353	5.74
Ni_3C/Ni@NF-8	1.263	5.66
Ni_3C/Ni@NF-350	0.9876	6.76
Ni_3C/Ni@NF-450	0.9543	6.31
Ni_3C/Ni@NF-550	1.478	11.80
RuO_2/NF	1.226	2.95
Bare NF	1.428	46.48

Table S6. Comparison of double layer capacitance (C_{dl}) and electrochemical active surface area (ECSA) of as-synthesized samples for OER.

Catalysts	C_{dl} (mF cm^{-2})	ECSA (cm^2)
Ni_3C/Ni@NF	63.95	1598.75
Ni@NF	33.29	832.25
Ni_3C/Ni@NF-0.5	28.38	709.50
Ni_3C/Ni@NF-8	14.53	363.25
Ni_3C/Ni@NF-350	53.09	1327.25
Ni_3C/Ni@NF-450	30.29	757.25
Ni_3C/Ni@NF-550	15.84	396.00
Bare NF	5.36	134.00

References

1 C. Feng, M. Lv, J. Shao, H. Wu, W. Zhou, S. Qi, C. Deng, X. Chai, H. Yang, Q. Hu and C. He, *Adv. Mater.*, 2023, **35**, 2305598.

2 X. Li, H. Zhang, Q. Hu, W. Zhou, J. Shao, X. Jiang, C. Feng, H. Yang and C. He, *Angew. Chem. Int. Ed. Engl.*, 2023, **62**, 202300478.

3 H. F. Yuan, S. M. Wang, Z. Z. Ma, M. Kundu, B. Tang, J. P. Li and X. G. Wang, *Chem. Eng. J.*, 2021, **404**, 126474.

4 S. Wang, Y. Zhang, X. Deng, Z. Ma, R. Cheng, Z. Wan, J. Li and X. Wang, *J. Mater. Chem. A*, 2023, **11**, 5222–5232.

5 Q. Hu, S. Qi, Q. Huo, Y. Zhao, J. Sun, X. Chen, M. Lv, W. Zhou, C. Feng, X. Chai, H. Yang and C. He, *J. Am. Chem. Soc.*, 2023, **146**, 2967–2976.

6 M. Zhang, W. Xu, T. Li, H. Zhu and Y. Zheng, *Inorg. Chem.*, 2020, **59**, 15467–15477.

7 H. Liu, Y. Zhang, R. Ge, J. M. Cairney, R. Zheng, A. Khan, S. Li, B. Liu, L. Dai and W. Li, *Appl. Energy*, 2023, **349**, 121582.

8 J. Kim, H. Jung, S. M. Jung, J. Hwang, D. Y. Kim, N. Lee, K. S. Kim, H. Kwon, Y. T. Kim, J. W. Han and J. K. Kim, *J. Am. Chem. Soc.*, 2020, **143**, 1399–1408.

9 L. Zhang, X. Wang, A. Li, X. Zheng, L. Peng, J. Huang, Z. Deng, H. Chen and Z. Wei, *J. Mater. Chem. A*, 2019, **7**, 17529–17535.

10 D. Li, L. Ding, Q. Zhao, F. Yang and S. Zhang, *Appl. Energy*, 2024, **356**, 122369.

11 J. Liu, Y. Gao, X. Tang, K. Zhan, B. Zhao, B. Y. Xia and Y. Yan, *J. Mater. Chem. A*, 2020, **8**, 19254–19261.

12 W. Zhou, Z. Xue, Q. Liu, Y. Li, J. Hu and G. Li, *ChemSusChem*, 2020, **13**, 5647–5653.

13 L. S. Wu, M. T. Zhang, Z. H. Wen and S. Q. Ci, *Chem. Eng. J.*, 2020, **399**, 125728.

14 D. Yan, L. Zhang, Z. Chen, W. Xiao and X. Yang, *Acta Phys. -Chim. Sin.*, 2020, **37**, 2009054.

15 X. Hu, T. Yang, Z. Yang, Z. Li, R. Wang, M. Li, G. Huang, B. Jiang, C. Xu and F. Pan, *J. Mater. Sci. Technol.*, 2022, **115**, 19–28.

16 B. Wang, Y. Chen, Q. Wu, Y. Lu, X. Zhang, X. Wang, B. Yu, D. Yang and W. Zhang, *J. Mater. Sci. Technol.*, 2021, **74**, 11–20.

17 G. Hou, X. Jia, H. Kang, X. Qiao, Y. Liu, Y. Li, X. Wu and W. Qin, *Appl. Catal. B*, 2022, **315**,

121551.

18 Y. T. Li, W. Ma, J. Wang and Q. Zhong, *J. Mater. Chem. A*, 2022, **10**, 24388–24397.

19 C. He, X. Hu, J. Wang, L. Bu, C. Zhan, B. Xu, L. Li, Y. Li and X. Huang, *Sci. China Mater.*, 2022, **65**, 3470–3478.

20 H. X. Chen, H. Xu, Z. R. Song, Y. Liu, H. Cui and J. K. Gao, *Rare Metals*, 2022, **42**, 155–164.

21 M. Sun, R. Ge, J. Yang, J. Qu, Y. Li, M. Zhu, J. M. Cairney, R. Zheng, S. Li and W. Li, *Appl. Energy*, 2022, **326**, 119999.

22 G. Liu, R. Yao, Y. Zhao, M. Wang, N. Li, Y. Li, X. Bo, J. Li and C. Zhao, *Nanoscale*, 2018, **10**, 3997–4003.